RESILIENT INFRASTRUCTURE
June 1–4, 2016
RESILIENT INFRASTRUCTURE LONDON 2016

ENHANCING THE DEFORMATION CAPACITY OF CONCRETE SHEAR WALLS REINFORCED WITH GFRP BARS

Ahmed Hassanein
Doctoral student, Université de Sherbrooke, Canada

Nayera Mohamed
Postdoctoral fellow, Université de Sherbrooke, Canada

Ahmed Sabry Farghaly
Postdoctoral fellow, Université de Sherbrooke, Canada

Brahim Benmokrane
Professor, Université de Sherbrooke, Canada
NSERC Research Chair in FRP Reinforcement for Concrete Infrastructure
Tier-1 Canada Research Chair in Advanced Composite Materials for Civil Structures

ABSTRACT

An experimental study was recently conducted to address the applicability of concrete shear walls entirely reinforced with glass-fiber-reinforced polymer (GFRP) bars and subjected to quasi-static reversed cyclic lateral loading in attaining reasonable strength and drift requirements specified in different codes. The reported test results clearly show that properly designed and detailed GFRP-reinforced concrete (RC) walls could reach their flexural capacities with no strength degradation. The results also demonstrate that the tested walls were able to achieve recoverable and self-centering behavior up to allowable drift limits before experiencing moderate damage and attain a maximum drift comparable to steel-RC walls. The promising results provide impetus for constructing shear walls with GFRP bars and constitute a step toward using GFRP bars in lateral-resisting systems. Since enhancing concrete confinement at the boundary might be a solution in attempting to increase the deformation capacity of GFRP-RC shear walls without significant loss of strength, a series of shear walls were constructed with different reinforcement confinement configurations at the boundary zone. This paper compares the first tested shear wall to a previously reported shear wall (Mohamed et al 2014a). The results show a significant increase in lateral drift and strength of almost 79% and 27%, respectively, by doubling the confinement reinforcement ratio of the boundary. The seismic behavior of the wall was obviously improved, and the deformability level was significantly enhanced.

Keywords: Concrete, GFRP bars, cyclic loads, hysteretic behavior, shear walls, drift, stiffness, deformability.

1. INTRODUCTION

Parking garages are one type of multistory building undergoing steel corrosion due to harsh climate conditions. Fiber-reinforced-polymer (FRP) bars have been innovatively used as reinforcement in many structural elements because of their corrosion resistance. As a new application for FRP reinforcement, full-scale shear walls reinforced with FRP bars under cyclic loading were recently tested as a primary lateral-resisting system typically used for parking garages. The results show that the FRP reinforced-concrete (RC) walls exhibited appropriate cyclic performance and possessed good deformation capacity in comparison to a steel-RC shear wall (Mohamed et al. 2014a). Mohamed et al. (2014a) carried out an experimental investigation of the applicability of reinforcing shear walls with GFRP bars in which the main parameters were steel versus GFRP reinforcing and different aspect ratios for GFRP-reinforced walls. The test matrix involved testing of four full-scale shear walls 3500 mm in height: one reinforced with steel bars and three with GFRP. Boundary-element reinforcement and diagonal bars were provided to eliminate sliding shear and ensure flexural domination. The test results show that all of the tested walls achieved

their predicted ultimate strength through flexural response, as evidenced by the typical amount of horizontal cracking. The observed failure mode was concrete crushing at one end associated with buckling of longitudinal bars for the steel reinforced wall and fracture of the longitudinal bars for the GFRP reinforced walls. The measured cyclic response of the GFRP-reinforced walls showed insignificant strength degradation and reasonable stability of stiffness. They achieved a higher drift ratio of 3.1% as compared to the steel wall's 2.6%. Due to FRP-bar brittleness, the GFRP RC-walls achieved a lower level of deformability than the steel-reinforced wall based on virtual yield-point analysis (Mohamed et al. 2014b).

In order to enhance the deformability behavior of GFRP walls, a series of five full-scale shear walls were constructed with different confinement configurations at the boundary zone with the aim of developing higher concrete strains at ultimate load and delaying the elastic–plastic transition point so as to possibly enhance the deformability performance of such walls. This paper investigates the cyclic response of the first wall tested and compares it to one of the walls tested by Mohamed et al. (2014a).

2. EXPERIMENTAL PROGRAM

The experimental program comprised the testing to failure of reinforced-concrete shear walls with a higher confinement configuration than that for the wall pre-tested by Mohamed et al. (2014a). They were designed with an adequate amount of distributed and concentrated reinforcement to ensure flexural domination and eliminate sliding and shear failures. The walls are classified as medium-rise walls according to CSA and ACI codes. The sections that follow describe specimen design and details, materials, instrumentation, and test setup.

2.1 Specimen Design and Details

The specimens represent a model of a single shear wall complying with the special seismic requirements specified in CSA A23.3 (2014) and ACI 318 (2008) for the seismic-force resisting systems (SFRSs), as a case for new unexamined SFRS (R_dR_o = 1). One GFRP-reinforced specimen (G15-II) was constructed and tested. The wall was analytically compared to the wall pre-tested by Mohamed et al. 2014a, referred to as G15-I. The minimum thickness and reinforcement details were according to CSA S806 (2012) and ACI 440.1R (2006). The wall specimens were 3500 mm high (h_w), 200 mm thick (b_w), and 1500 mm long (l_w), resulting in a shear-wall aspect ratio (h_w/l_w) of 2.3. Figure 1 shows the concrete dimensions and reinforcement details of the shear-wall specimens.

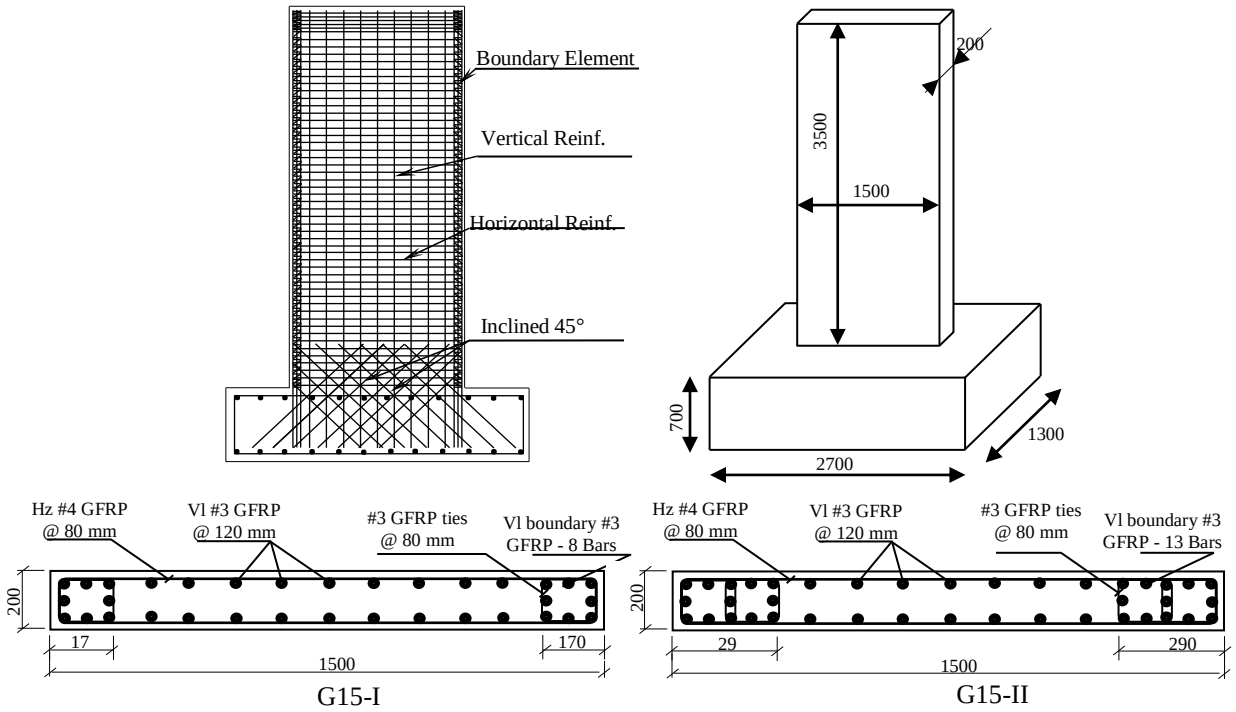

Figure 1: Concrete dimensions and reinforcement details

The reinforcement details of the GFRP reinforcement specimens (G15-I and G15-II) complied with CSA S806 (2012) minimum reinforcement requirements, resulting in two layers of vertical reinforcement comprised of #3 (10 mm diameter, A_f = 71.3 mm^2) GFRP bars spaced at 120 mm. Eight #3 GFRP bars were used as vertical reinforcement for each boundary element on both side ends of G15-I, while 13 #3 GFRP bars were used in the boundary of G15-II. The boundaries were tied with GFRP #3 rectangular spiral stirrups (140 × 140 mm for G15-I and 140 × 260 mm for G15-II) spaced at 80 mm, which is approximately the maximum spacing permitted in CSA S806 (2012) (75 mm). The web horizontal reinforcement consisted of two layers of #4 (13 mm diameter, A_f = 126.7 mm^2) GFRP bars spaced at 80 mm. Table 1 lists the reinforcement ratios for the tested walls. The ultimate lateral load (V_f) was predicted based on plane sectional analysis. Table 1 lists the predicted values.

Table 1: Reinforcement details and calculated capacities of the walls

Wall	f'_c (MPa)	Reinforcement Ratio				P_u (kN)	V_r (kN)	V_f (kN)	P_u/V_f
		ρ_v	ρ_h	ρ_l	ρ_t				
G15-I	39.9	0.58	1.58	1.43	0.89	586	884	563	1.04
G15-II	33.0	0.54	1.58	0.67		745	879	725	1.03

f'_c = concrete compressive strength; V_f = predicted load
ρ_v = web vertical-bar reinforcement ratio; ρ_h = web horizontal-bar reinforcement ratio
ρ_l = boundary longitudinal-bar reinforcement ratio; ρ_t = boundary tie reinforcement ratio
P_u = experimental ultimate lateral load; V_r = factored shear strength

Sufficient shear reinforcement was provided to resist the shear force associated with the development of the probable moment resistance of the tested walls. The factored shear strength (V_r) of a reinforced-concrete cross section is the sum of the shear resistance provided by the concrete and shear reinforcement. Using the described detailed reinforcement, the factored shear strength of the walls was calculated based on the sectional analysis equations in CSA S806 (sections 8.4.4.5 to 8.4.4.11), resulting in a V_f/V_r of not more than 0.75, as listed in Table 1.

2.2 Material Properties

All specimens were constructed with normal-weight, ready-mixed concrete having a nominal compressive strength (f_c') of 40 MPa. Table 1 gives the actual concrete compressive strength based on the average values from tests performed on at least five 100 × 200 mm cylinders for each concrete batch on one day before testing. The GFRP reinforcing bars were two diameters of high-modulus (HM) sand-coated bars (CSA S807 2010): #3 for vertical bars (f_{fu} = 1412 MPa, E_f = 66.9 GPa, ε_{fu} = 2.11%, A_f = 71.3 mm^2) and spiral ties (for straight portions: f_{fu} = 962 MPa, E_f = 52 GPa, ε_{fu} = 1.85%, A_f = 71.3 mm^2; for bent portions: f_{fu} = 500 MPa) and #4 for horizontal bars (f_{fu} = 1392 MPa, E_f = 69.6 GPa, ε_{fu} = 2%, A_f = 126.7 mm^2). The longitudinal tensile properties of the FRP bars were determined by testing five specimens according to ASTM D7205 (2011) for straight bars and test method B.5 in ACI 440.3R (2004) for bent bars.

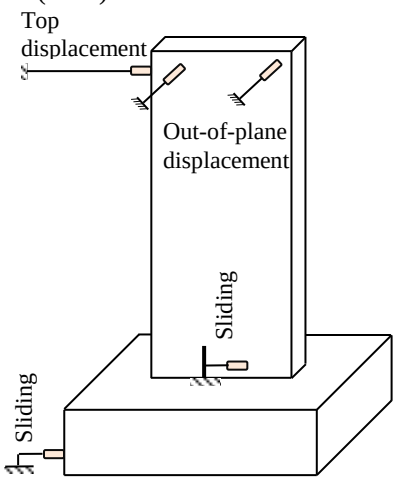

Figure 2: Instrumentation

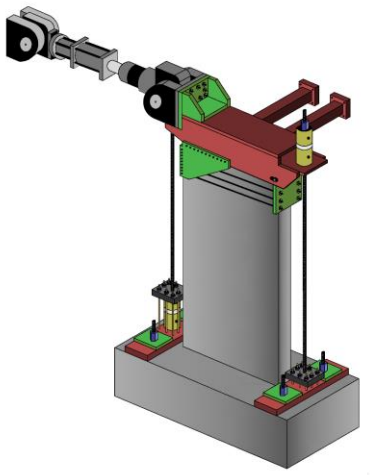

Figure 3: Test setup

2.3 Test Setup and Procedure

A series of linear variable differential transducers (LVDTs) and strain gauges were used to measure critical response quantities. That notwithstanding, only the instruments used in this study will be shown (Figure 2). Lateral displacement was measured at the top of the wall height; two LVDTs were used to measure horizontal sliding between the wall and base slab as well as between the base slab and rigid floor (unlikely to occur). An automatic data-acquisition system monitored by a computer was used to record the LVDT and load-cell readings. During loading, crack formation was marked and recorded.

Figure 3 shows the test setup. The wall specimens were tested in an upright position. A specially fabricated steel load-transfer assembly was used to transfer both axial and lateral loads to the wall specimen. An axial load of approximately $0.07 b_w . l_w . f_c'$ was applied at the top of the wall by two hydraulic jacks mounted to the load-transfer assembly. The axial stress was maintained constant throughout the duration of each test. Cyclic lateral displacements were applied to the walls with a 1000 kN MTS actuator mounted horizontally to a reaction wall. Out-of-plane bracing was provided to prevent out-of-plane displacement, simultaneously providing no resistance to in-plane displacement. As the loading history was not a test variable, a typical procedure of applying quasi-static reversed cyclic loading until failure was used (Figure 4). The walls were cycled twice at each displacement level with increments of 2 mm up to 10 mm, followed by increments of 5 mm up to 50 mm, and then increments of 10 mm to failure. Hinged connections at the tips of both the horizontal actuator and vertical hydraulic jacks prevented any substantial restraint of rotation of the top of the wall, thus ensuring cantilever behavior.

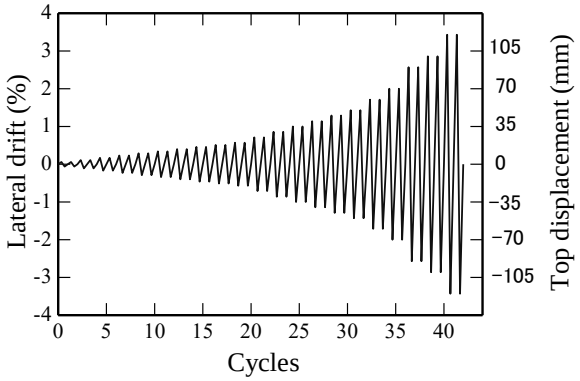

Figure 4: Applied displacement history

3. EXPERIMENTAL RESULTS

3.1 General Behavior

In general, each wall exhibited a reasonably symmetric lateral load–top displacement relationship for loading in the +ve and -ve directions until boundary concrete crushing occurred at one end. The behavior of both walls was dominated by a flexural response, as evidenced by the typical amount of horizontal cracking shown in Figure 5. No sign of premature shear, sliding shear (no sliding displacement was measured), or anchorage failure was observed. Under increased displacement, horizontal cracks continued to form up to a height of approximately *2/3* h_w in G15-I and more than *3/4* h_w in G15-II. The horizontal cracks extended in a downward trend inside the web forming diagonal cracks. As loading continued, vertical splitting cracks typically appeared in the walls at the boundary under compression. With increased displacement, spalling of the concrete cover became more significant at the compression end of the walls (Figure 6). Thereafter, wall stiffness decreased as a result of crack spreading, but the lateral load kept increasing.

G15-I continued to carry load in each cycle with no degradation until concrete crushing and fracture of the longitudinal GFRP bars, followed by rupture of the GFRP ties (Figure 7). G15-II, however, experienced no failure as the hysteretic response demonstrated a horizontal plateau at a drift level of 4.89 % until reaching the maximum displacement capacity of the actuator. Subsequently, the test was stopped before the failure of the wall specimen. Table 2 summarizes the failure progression of the tested specimens.

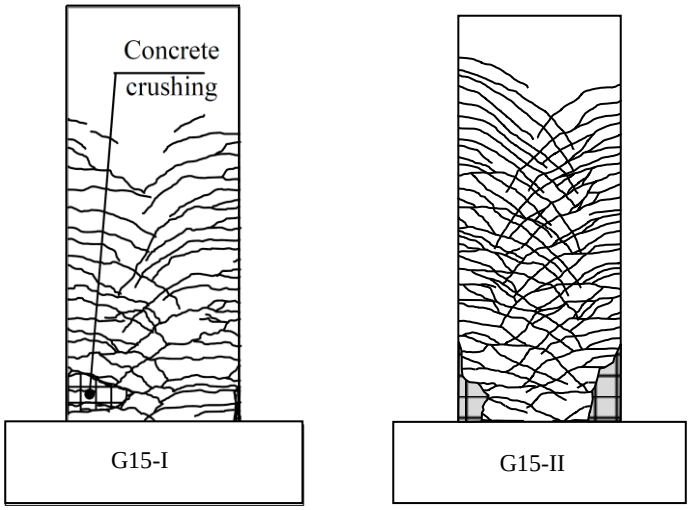

Figure 5: Crack pattern

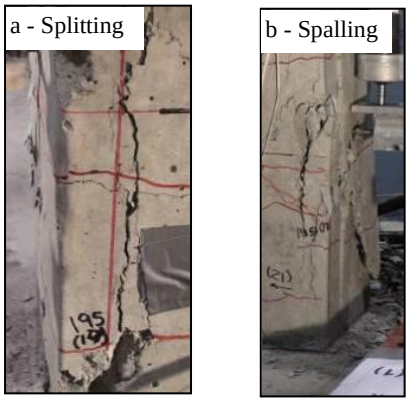

Figure 6: Splitting and spalling of concrete cover

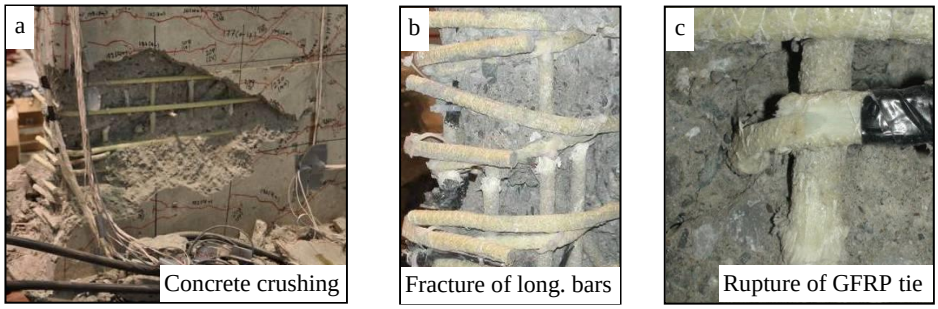

Figure 7: Failure of G15-I

Table 2: Failure progression

	Stage	First Crack	Flex–Shear Crack	Vertical Spalling	Concrete Crushing	Maximum Load
G15-I	*P* (kN)	162	193	437	586	586
	Δ (mm)	7.6	12.9	68	108	108
	Drift (%)	0.22	0.37	1.9	3.1	3.1
G15-II	*P* (kN)	147	219	440	-	745
	Δ (mm)	5.7	15.0	70	-	194.6
	Drift (%)	0.16	0.43	2.0	-	5.6

Overall, both walls achieved their flexural strength, as shown in Table 1. The following sections provide information on the lateral load–top displacement relationship, extent of damage, and the energy dissipation for each wall.

3.2 Hysteretic Response

Both walls showed a pinched behavior of hysteresis loops with no strength degradation, as shown in Figure 8. The unloading/reloading curves seemed to demonstrate linearity depending on GFRP elastic behavior. The reloading branches followed a similar loading path but at a lower loading stiffness, resulting in lower peak strength. The shape of the unloading path seems to be dependent on the strain at the onset of unloading. The lateral load–top displacement curves indicate that the first cycle of a new displacement level followed the loading path of the second cycle at the previous displacement level. This suggests that additional cycles at a specific displacement level would produce negligible damage in comparison to that experienced in the first unloading/reloading cycle.

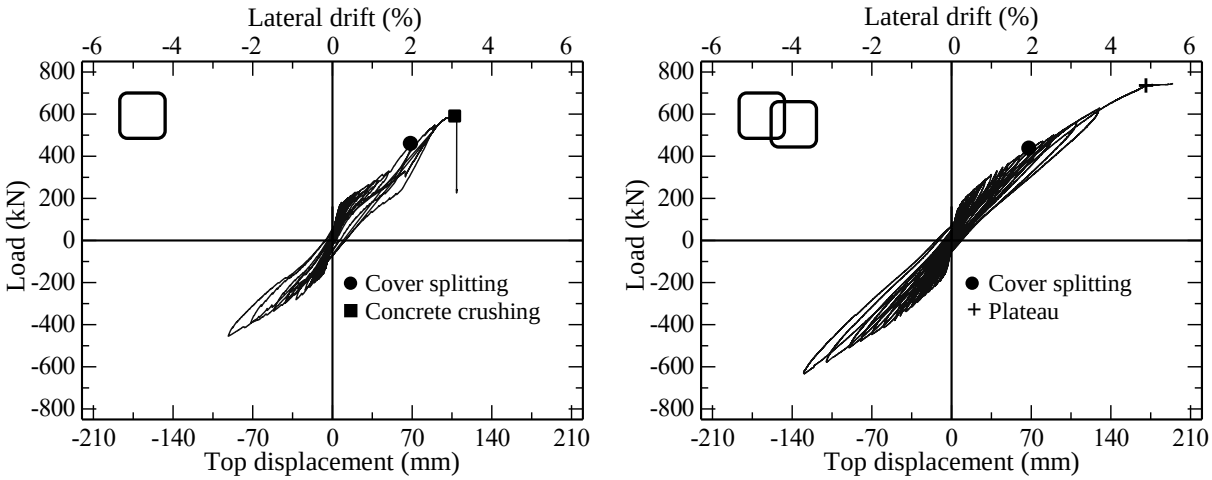

(a) G15-I (Mohamed et al. 2014a) (b) G15-II

Figure 8: Hysteretic response

The hysteretic response observed for G15-II exhibits more pinching loading/unloading loops than that for G15-I but with a similar initial stiffness, as shown in Figure 8. An initial linear branch corresponding to the uncracked condition of the wall is evident. At a lateral drift of 0.22%, a crack initiated, reducing stiffness with initial crack widths of 0.125 and 0.137 mm for G15-I and G15-II, respectively. As the lateral load increased, the walls exhibited a softened response, with the propagation of cracks that closed and realigned after each cycle. The same pattern continued with increased deformations up to lateral drifts of 1.43 % to 1.6%, at which point all crack propagation stabilized. Vertical cover splitting in the boundary gradually initiated at the most heavily compressed fibers (Figure 6-a) at approximately 2% of lateral drift. At a lateral drift of 2.6%, spalling of the concrete cover took place at the boundary element (Figure 6-b). With increasing lateral load, concrete crushing (Figure 7-a) associated with the rupture of the GFRP ties (Figure 7-b) was clearly evident, causing wall failure and a drop in strength, followed by the sequential rupture of the GFRP bars in the boundary under compression (Figure 7-c). In subsequent cycles of G15-II, the hysteretic response demonstrated a horizontal plateau at a drift level of 4.89 % with a constant load level until reaching a drift level of 5.6%. At that point, the maximum displacement capacity of the MTS actuator was

reached before the wall specimen failed, so the test was stopped. The ultimate lateral loads attained were 586 and 745 kN, corresponding to lateral drifts of 3.1 % and 5.6% for G15-I and G15-II, respectively.

3.3 Envelope Curve

Figure 9 shows the envelope curves for both walls. It is clear that both walls behaved similarly. It is interesting to note that the concrete cover of both walls split—considered moderate damage—at similar loads and drift levels (see Table 2). The drift values fell within the range of 1.5 % to 2% (reached with moderate damage to both walls), which is the recommended allowable design drift in many codes (CSA A23.3 2014 and Duffey et al. 1994). After that point, both walls kept increasing almost linearly until G15-I failed at a load of 586 kN, corresponding to 3.1% drift. G15-II, however, reached a higher load, corresponding to a higher drift level, which can be attributed to the confinement effect.

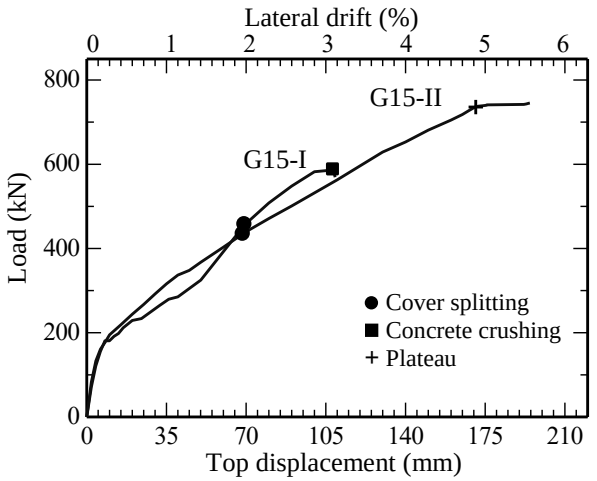

Figure 9: Envelope curve

Generally, both walls evidenced minimal crack width and ability to recover and realign cracking up to a lateral drift of 2%, which is considered an advantage in using GFRP bars and provides proof of sufficient bond between the concrete and GFRP bars (Mohamed et al. 2014a). For many years, engineers believed that hysteretic pinching was an undesirable characteristic that would lead to larger structural displacements during inelastic response. Recent research (Huang and Foutch 2009, Sharbatdar and Saatcioglu 2009), however, has indicated that hysteretic pinching without strength degradation does not produce undesirable responses and can result in less structural deformation than elastic–perfectly plastic behavior. Therefore, the behavior of GFRP-reinforced shear walls can be accepted in resisting lateral forces. Moreover, increasing the confinement level of the wall's boundary elements (G15-I) resulted in a higher lateral drift with the presence of a horizontal plateau.

3.4 Secant Stiffness

Realistic modeling of RC buildings with shear walls typically dictates the use of relatively simple elements for all members, preferably using one element for each structural member. In this typical situation, it is essential to use realistic values for the stiffness of the wall elements, which are known to be significantly lower than that corresponding to gross-section properties, even at the serviceability limit state (Aktan et al. 1985).

The stiffness properties of the walls tested were assessed with their secant stiffness, defined as the ratio of peak load of each cycle to the corresponding displacement. As a result, the stiffness degradation during cycling at a constant displacement can also be assessed. Figure 10 shows the K_i/K_0 of the secant stiffness at various levels of lateral drift to the initial stiffness of wall specimens. As expected, considerable reduction in stiffness took place in the specimens as higher levels of deformation were imposed. The decreased stiffness resulted in apparent strength degradation, that is, the same displacement amplitude was reached at a higher force. Both walls had almost identical stiffness ratios at

the different drift levels. It is clear that the confinement did not enhance the stiffness ratio. Moreover, the achieved stiffness ratios at the moderate-damage level (corresponding to 2% of lateral drift) were similar in both walls.

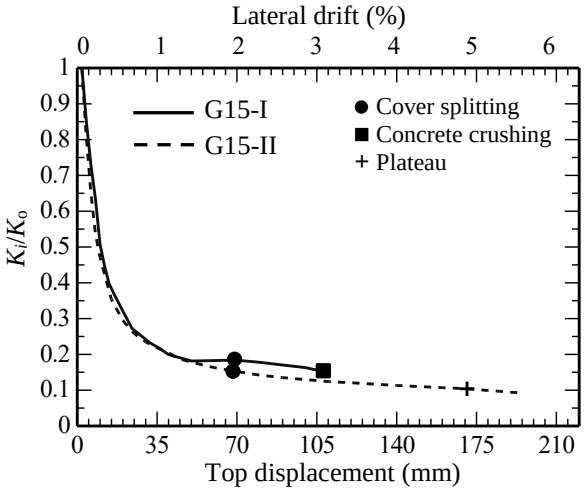

Figure 10: Ratio of secant to initial stiffness

4. DEFORMATION CAPACITY

Ductility is a measure of the ability of the wall to deform beyond yielding of the flexural reinforcement. As FRP bars do not yield (they are elastic), Jaeger et al. (1995) proposed the new term "deformability" to describe a comparison method based on deformability and strength considerations instead of ductility. Since concrete members reinforced with FRP bars are highly deformable, structures should be designed based on a curvature factor, as curvature is the double integration of deflection. The curvature factor is the ratio of curvature at the ultimate state to the curvature at a concrete strain of 0.001. Moreover, Jaeger et al. (1995) suggested considering the strength factor, which is defined as the ratio of ultimate moment to moment at a concrete strain of 0.001. To take these two capacities into account, Jaeger et al. (1995) defined an overall deformability factor (*J*) calculated as the product of the curvature factor and strength factor expressed as follows:

[1] $$J = \frac{M_u}{M_c}\frac{\phi_u}{\phi_c}$$

where *M* and Φ are moment and curvature at service or ultimate load, denoted by the subscripts *c* or *u*, respectively. The *Canadian Highway Bridge Design Code* (CHBDC) includes an overall performance factor for FRP-RC beams and slabs (CSA S6S1-10) that combines the strength and deformability given by Eq. 1 with the service condition taken as the point at which the maximum concrete compressive strain reaches 0.001.

The 0.001 concrete compression-strain limit was chosen to represent linear stress–strain behavior in compression and defined the serviceability limit state. The concrete compression strain of G15-II reached more than 0.015 at the maximum load. Mohamed et al. (2014a) reported a concrete compression strain of 0.007 at ultimate load; the concrete compression-strain limit of 0.001 is very conservative compared to the actual test values. Therefore, the deformability factor (*J*) was recalculated for moment and curvature values corresponding to a concrete compressive strain equal to 0.0035. Table 3 provides the calculated values of the deformability factor (*J*) for G15-II versus G15-I reported by Mohamed et al. (2015).

Table 1: Deformability factor

Wall	$J_{0.001}$	$J_{0.035}$
G15-I	22.0	2.10
G15-II	86.6	8.62

The deformability factor (J) was calculated and resulted in unreliably high values (referred as $J_{0.001}$ in Table 3). As the moment and curvature were determined at a concrete compressive strain of 0.001 (the recommended value for FRP-RC beams and slabs according to the CHBDC), high values of $J_{0.001}$ were reached due to well-confined concrete, which allowed the concrete compressive strain to reach more than 0.007 at ultimate load (Mohamed et al. 2014a). Therefore, the deformability factor J was recalculated for moment and curvature values corresponding to a concrete compressive strain of 0.0035 ($J_{0.0035}$). Table 3 lists the original $J_{0.001}$ and modified $J_{0.0035}$ deformability factor resulting in a large difference between the two procedures due to the difference in the values of moments and curvatures corresponding to concrete compressive strains of 0.001 and 0.0035. The calculated $J_{0.0035}$, however, provided more reliable values.

5. CONCLUSIONS

The main aspects that were investigated by means of these tests concern the effects of the reinforcement content and configuration in the boundary element on the deformation behavior of the tested walls. G15-II, which had double overlapped ties in the boundary element evidenced significant enhancement in deformation capacity compared to G15-I with one tie. The maximum drift ratio and maximum lateral load of G15-II were 79% and 27% higher than those of G15-I, respectively. The predicted flexural strength was in close agreement with the measured load-carrying capacities. In general, the hysteresis response, stiffness degradation, and energy dissipation of both walls were very similar, which shows that GFRP-reinforced shear walls can demonstrate a predictable linear behavior up to failure.

ACKNOWLEDGMENTS

The authors wish to acknowledge the financial support of the Natural Sciences and Engineering Research Council of Canada (NSERC), the Canada Research Chair in Advanced Composite Materials for Civil Engineering, and the Fonds québécois de la recherche – Nature et Technologies - (FQRNT) of Quebec.

REFERENCES

ACI Committee 318 2008. Building Code Requirements for Structural Concrete and Commentary (ACI 318-08). *American Concrete Institute*, Farmington Hills, MI, 473 pp.

ACI Committee 440 2006. Guide for the Design and Construction of Concrete Reinforced with FRP Bars (ACI 440.1R-06). *American Concrete Institute*, Farmington Hills, MI, 44 pp.

ACI Committee 440 2004. Guide Test Methods for Fiber-Reinforced Polymers (FRPs) for Reinforcing or Strengthening Concrete Structures (ACI 440.3R-04). *American Concrete Institute*, Farmington Hills, MI, 40 pp.

Aktan, A. E., Bertero, V. V. and Sakino, K. 1985. Lateral Stiffness Characteristics of Reinforced Concrete Frame-Wall Structures. *ACI SP-86*: *Deflections of Concrete Structures*, 231-262.

ASTM D7205 / D7205M – 06. 2011. Standard Test Method for Tensile Properties of Fiber Reinforced Polymer Matrix Composite Bars.

CSA A23.3 2014. Design of Concrete Structures Standard. *Canadian Standards Association*, Mississauga, Ontario, Canada, 240 pp.

CSA S806 2012. Design and Construction of Building Components with Fiber-Reinforced Polymers. *Canadian Standards Association*, Mississauga, Ontario, Canada, 208 pp.

CSA-S6-06. 2010. Supplement #1 to Canadian Highway Bridge Design Code (CAN/CSA S6S1-10), *Canadian Standards Association*, Mississauga, Ontario, Canada, 1078 pp.

Duffey, T.A., Farrar, C.R. and Goldman A. 1994. Low-Rise Shear Wall Ultimate Drift Limit. *Earthquake Spectra*, 10 (4): 655-674.

Huang, Z. and Foutch, D. A. 2009. Effect of Hysteresis Type on Drift Limit for Global Collapse of Moment Frame Structures under Seismic Loads. *Journal of Earthquake Engineering*, 13 (7): 939-964.

Jaeger L.G., Tadros G. and Mufti A.A. 1995. Balanced Section, Ductility and Deformability in Concrete with FRP Reinforcement. *Technical Report No. 2-1995, CAD/CAM Centre*. Technical University of Nova Scotia, Halifax.

Mohamed, N., Farghaly, A. S., Benmokrane, B. and Neale, K. W. 2014a. Experimental Investigation of Concrete Shear Walls Reinforced with Glass-Fiber-Reinforced Bars under Lateral Cyclic Loading. *ASCE Journal of Composites for Constructions*, 18 (3): 04014001.

Mohamed, N., Farghaly, A. S., Benmokrane, B. and Neale, K. 2014b. Drift Capacity Design of Shear Walls Reinforced with GFRP Bars. *ACI Structural Journal*, 111 (6): 1397-1406.

Mohamed, N., Farghaly, A. S. and Benmokrane, B. 2015. Aspects of Deformability of Concrete Shear Walls Reinforced with Glass–Fiber–Reinforced Bars. *ASCE Journal of Composites for Constructions*, 19 (5): 06014001.

Sharbatdar, M. K. and Saatcioglu, M. 2009. Seismic Design of FRP Reinforced Concrete Structures. *Asian Journal of Applied Science*, 2 (3): 211-222.